TECHNICAL RESEARCH REPORT

SYSTEMS RESEARCH CENTER

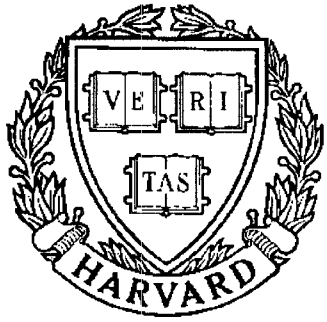

Supported by the National Science Foundation Engineering Research Center Program (NSFD CD 8803012), the University of Maryland, Harvard University, and Industry

Comparative Study of Friction-Compensating Control Strategies for Servomechanisms

by N.E. Leonard and P.S. Krishnaprasad

TR 91-88

Comparative Study of Friction-Compensating Control Strategies for Servomechanisms *

Naomi Ehrich Leonard and P. S. Krishnaprasad

Electrical Engineering Department
&
Systems Research Center
University of Maryland
College Park, MD 20742

Abstract

This paper describes a comparative investigation of friction-compensating control strategies designed to improve low-velocity position tracking performance for servomechanisms. Several control methods are considered including adaptive control and estimation-based control. Additionally, the various controller designs incorporate different friction models ranging from classical friction and Stribeck friction to the less popular Dahl friction model. This investigation of friction models is motivated by the fact that there is little consensus in the literature on how best to model friction for dynamic friction compensation. The control strategies are compared in an extensive test program involving position tracking experiments on a direct-drive dc motor. This effort addresses the

*This research was supported in part by the National Science Foundation's Engineering Research Centers Program: NSFD CDR 8803012 and by the AFOSR University Research Initiative Program under grant AFOSR-90-0105.

current lack of comparative experimental results on friction compensation. The results show that the adaptive and estimation-based controllers outperform more traditional linear controllers. The experiments also yield insight into the appropriateness of the different friction models under the tested operating conditions. In particular, the Dahl model is observed to provide a reliable representation of friction behavior near zero velocity.

1 Introduction

Recent growth in the number and variety of robotics applications has led to a demand for increased precision in robotic manipulation. However, robotic manipulators must contend with friction which poses a serious challenge to precise manipulator control. Specifically, failing to compensate for friction can lead to tracking errors when velocity reversals are demanded and oscillations when very small motions are required. To compensate for friction it is best to have some knowledge of the structure of friction, yet there is little overall agreement in the literature on how best to model friction. Further, friction compensation is complicated by the fact that friction parameters vary with temperature and age.

Traditionally, control engineers have used open-loop smoothing techniques, such as dither and pulse-width modulation, to compensate for friction in mechanical systems. However, these techniques have disadvantages, for example, dither can cause mechanical problems such as fatigue by exciting vibrations in manipulators.

As an alternative to these techniques, researchers in control engineering have recently considered adaptive and estimation-based control techniques for compensation of friction in mechanical systems [Gilbart and Winston, 1974, Walrath, 1984, Craig, 1988, Canudas et al., 1986]. Among the compensators

proposed in the literature, a variety of friction models are assumed. Much of this work shows experimental evidence that a particular friction model together with a suitable compensation technique improves system performance. However, since each research team performed different experiments, there is no easy way to compare the relative effectiveness of the different control-technique and friction-model combinations.

This paper provides experimental results that indicate the relative effectiveness of five different friction-compensating controllers. Of the five controllers tested, two are modified versions of adaptive controllers designed by [Gilbart and Winston, 1974] and [Craig, 1988], respectively. Each assumes the classical model of friction. *However, in the present study both adaptive controllers have been upgraded to include more detailed friction elements such as asymmetries and Stribeck friction.*

The third controller tested is a modified version of the estimation-based friction-compensating controller of [Walrath, 1984]. This controller design is based on the Dahl friction model which predicts a first-order dynamic model of friction as a function of displacement with a time constant that is a linear function of velocity. Whereas Walrath was unable to experimentally derive this linear time constant function, the experiments described in this paper successfully verify Dahl's prediction. Additionally, an original stability proof for the estimation-based controller that uses the passivity formalism is outlined in this paper.

The fourth controller tested is a linear controller with dither. This controller is included as a sample smoothing controller. The benchmark for the test program is a conventional linear controller with optimized proportional, integral, and derivative (PID) gains.

The experimental program, designed for the hardware available in the laboratory, provides a realistic servomechanism control problem. The subject of the program is a direct-drive brush-type dc motor, digitally controlled by means of an IBM AT personal computer (PC). The same series of position tracking experiments are performed on the motor with each of the five controllers. The experiments involve position trajectory tracking with velocity reversals which exercise the problems associated with friction at near-zero velocities and the discontinuous nature of friction at zero velocity. Tracking performance is measured by root-mean-square (RMS) position error which provides some averaging of external effects. Nonetheless, unmodelled effects such as torque ripple and digital sampling rate are addressed with additional experimentation.

Section 2 of this paper describes the different models of friction found in the literature with a discussion of how each feature of friction influences servomechanism dynamics. Section 3 discusses friction-compensating control strategies and presents the design of the adaptive and estimation-based controllers tested experimentally. Section 4 provides the details of the experimental program and the experimental results. Conclusions along with some suggestions for future work are given in Section 5.

2 Friction Structure and Dynamics

Using both theory and experimentation, researchers in a number of fields have developed several different models of the structure and dynamics of friction. In selecting a friction model for our dynamic friction-compensating control problem, it is important to consider how the various identified features of friction influence the dynamics of a servomechanism.

Although rolling friction is a physically different phenomenon from rubbing

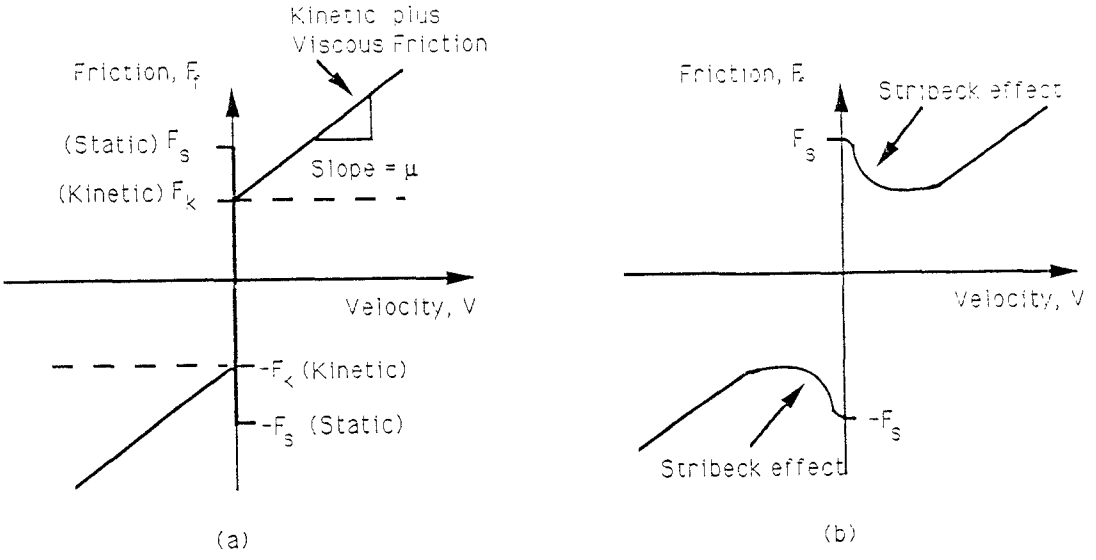

Figure 1: (a) Classical Model of Static, Kinetic and Viscous Friction and (b) Stribeck Friction

or sliding friction, the models discussed below attempt to describe the dynamics of a system with rolling *or* sliding friction. Pure rolling friction conditions occur when the contact between two surfaces is a point. However, according to [Rabinowicz, 1965], the contact region between two surfaces is typically of larger area than a point because of elastic (and possibly plastic) deformation on one or both of the surfaces. The resulting "rolling" friction in this case involves a combination of sliding and pure rolling friction. In fact, although the sliding velocity is usually small compared to the rolling velocity, sliding friction often provides the major component of the total friction. Consequently, it is appropriate to consider the same models for sliding friction and "rolling" friction.

Classical friction is the earliest and most widely used model of friction. The three components of classical friction: kinetic friction, viscous friction, and static friction, are illustrated on the friction versus velocity graph of Figure 1(a). Although kinetic friction simply provides a constant retarding force to rubbing surfaces, it also introduces a discontinuity at zero velocity. As a result,

servomechanisms performing bi-directional tasks will be subject to the discontinuity during every velocity reversal. The discontinuous behavior of kinetic friction can be classified as a "hard nonlinearity". It is well-known that a closed loop system with a hard nonlinearity can produce a limit cycle, i.e., self-sustained oscillations, that would cause poor control accuracy.

Viscous friction results from the viscous behavior of a fluid lubricant layer between two rubbing surfaces. As shown in Figure 1(a), viscous friction is represented as a linear function of velocity.

Static friction is the force required to initiate motion from rest. Typically, the magnitude of static friction is greater than the magnitude of kinetic friction which can lead to intermittent motion known as "stick-slip". Stick-slip manifests itself as repeated sequences of sticking between two surfaces with static friction followed by sliding or slipping of the two surfaces with kinetic friction. For the servomechanism control problem, stick-slip can diminish control accuracy. The stick-slip cycling can be avoided if damping and stiffness are sufficiently high.

The classical lumped friction model F_f of static friction F_s, kinetic friction F_k, and viscous friction, which depend on the applied tangential force F, velocity V, and coefficient of viscous friction μ, is as follows:

$$F_f = \begin{cases} F_k sgn(V) + \mu V & \text{if } V \neq 0 \\ F_s sgn(F) & \text{if } V = 0 \end{cases} \tag{1}$$

Some experimentalists have noted that in machines with rubbing parts more complicated and numerous than a single body sliding over a second body, the magnitudes of kinetic, viscous, and static friction are not the same in the positive and negative directions [Canudas et al., 1986, Armstrong-Hélouvry, 1991, Wang, 1987]. A more general model of friction that accounts for this asymmetry uses different friction coefficients in the positive and negative directions.

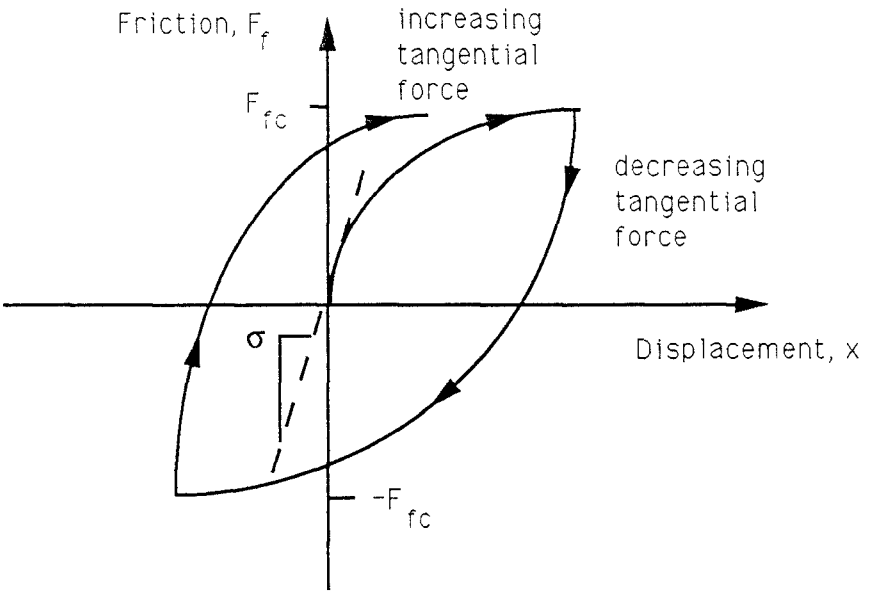

Figure 2: Pre-Sliding Displacement Phenomenon (Dahl Effect)

Contrary to the predictions derived from the classical friction model, researchers including the authors of [Courtney-Pratt and Eisner, 1957] and others have found that small relative displacements between two bodies in contact do occur when the applied relative tangential force is *less* than the static friction. This pre-sliding displacement phenomenon is illustrated in Figure 2 which shows friction F_f as a function of displacement x based on experimental results.

In [Dahl, 1977] the author provided a model of the pre-sliding displacement phenomenon, known as the "Dahl model", that assumes friction F_f is a function of displacement x and time t such that

$$\frac{dF_f(x,t)}{dt} = \frac{\partial F_f(x,t)}{\partial x} \cdot \dot{x} + \frac{\partial F_f(x,t)}{\partial t} , \tag{2}$$

with $\partial F_f/\partial t = 0$, and

$$\frac{\partial F_f(x,t)}{\partial x} = \sigma |1 - \frac{F_f}{F_{f_c}} sgn(\dot{x})|^i . \tag{3}$$

σ and F_{f_c} are as shown in Figure 2, and i is an exponent parameter that Dahl empirically derived to be $i \approx 1.5$.

A friction-compensating adaptive controller based on Dahl's model was designed and successfully used for the stabilization of an airborne pointing and tracking system [Walrath, 1984]. Walrath found from experimentation that friction responds continuously to velocity reversals. Using the classical discontinuous static-kinetic friction model, Walrath could not re-create this smooth behavior. Dahl's model, on the other hand, predicted the expected smooth behavior.

The classical friction model predicts behavior more characteristic of a system that spends longer periods of time at zero velocity. Specifically, the magnitude of static friction is dependent on the length of time the surfaces are at rest, i.e., the "dwell time". This static friction dependence on dwell time explains why under stick-slip conditions the amplitude of the stick-slip limit cycle is observed to decrease with increasing velocity.

While the simple static plus kinetic friction model offers an intuitive explanation for the possibility of stick-slip oscillations, it inadequately justifies the existence of these limit cycles for all the conditions under which they have been observed. However, several researchers, e.g., [Armstrong-Hélouvry, 1991] have experimentally confirmed that friction varies with velocity as depicted in Figure 1(b). The implications of the Stribeck effect with regard to servomechanism dynamics include an increased likelihood of stick-slip limit cycling at low velocities. Of the many empirical models derived for friction incorporating the Stribeck effect, the following is the most popular:

$$F_f(V) = F_k sgn(V) + \mu V + (F_s - F_k)e^{-(V/V_{str})^2} sgn(V) \; . \tag{4}$$

where V_{str} is the critical Stribeck velocity.

Frictional lag is one other feature of friction that may also have a significant impact on dynamics. While we do not consider this in the present study, we note the considerable empirical evidence that has recently become available indicating

that friction does not respond instantaneously to a change in velocity. The primary work here is due to geophysicists [Rice and Ruina, 1983] who use stick-slip for earthquake-related predictions. Hess and Soom [Hess and Soom, 1990] also found strong evidence of frictional lag, in their experiments on a flat steel button rubbing against a rotating steel disk. Frictional lag makes stick-slip instabilities less likely. Because a decrease in friction occurs *slowly* when velocity is increased, stiff systems will not experience stick-slip [Armstrong-Hélouvry, 1991]. We hope to investigate these aspects in future work.

3 Friction-Compensating Control

If a system with friction is linear and is to be operated only at relatively high velocities without changing directions, i.e., without crossing zero velocity, friction can be modelled as a linear function of velocity. Under these conditions, standard PID design techniques can be applied to the dynamics of the linear system plus viscous friction with reliable results. On the other hand, if the system is to be operated at low velocities or with direction reversals, then the standard PID design techniques may be unsuitable and tracking accuracy may prove inadequate. Additionally, to prevent limit cycling due to the static-kinetic friction discontinuity at zero velocity or the Stribeck effect, a PID controller must have sufficiently high "damping" K_d and "stiffness" K_p. However, high gain control has its own practical disadvantages such as introducing instability in a compliant drive train or saturating an actuator.

One popular alternative is the use of a technique such as dither which transforms the dynamics of a system with a discontinuity into smooth dynamics that can be more easily controlled with standard techniques. Dither is a high frequency signal added to the error signal in a feedback loop before it is input to the system. If the frequency is chosen to be higher than the cut-off frequency

of the system, the high-frequency behavior is filtered out leaving only the low-frequency "average" response.

Pulse-width modulation is another commonly used and effective smoothing technique that also works on the principle of averaging. However, both dither and pulse-width modulation have inherent disadvantages. For example, analysis and prediction of system characteristics such as stability and robustness are difficult to perform when dither or pulse-width modulation is applied. Additionally, dither can cause mechanical problems in a system such as a robot by exciting vibrations.

Friction-compensating adaptive and estimation-based controllers are nonlinear controllers that can be designed to take advantage of what is known about the structure of friction. Adaptive control strategies, in particular, are naturally suited to the problem of friction compensation because they generate a time-varying control law that tracks slowly varying system parameters, and they provide system identification when an accurate system model is not available. Three adaptive and estimation-based controllers are investigated in this paper.

For reference, the dynamics of the dc motor used in this paper are described by

$$\ddot{\theta}_p(t) + c_1\dot{\theta}_p(t) = -c_2T_f + c_3u(t) \ , \tag{5}$$

where θ_p, $\dot{\theta}_p$, $\ddot{\theta}_p$ are plant angular position, velocity, and acceleration, T_f is the friction and may depend on θ_p, $\dot{\theta}_p$, etc., u is the control input, and c_1, c_2, c_3 are constants (c_1 includes viscous friction).

The first of the adaptive and estimation-based controllers is an adaptive controller (referred to as AEC I) based on the Model Reference Adaptive Control (MRAC) approach proposed by [Gilbart and Winston, 1974] in their work on control of a satellite-tracking telescope. However, while Gilbart and Winston considered velocity trajectory tracking in their design, the controller in the

present paper was required to handle position trajectory tracking. As a result, AEC I is a modified version of the Gilbart and Winston design, incorporating filters to reduce the order of the system.

Additionally, Gilbart and Winston assumed the classical, symmetrical kinetic plus viscous friction model in the dynamic system equations. To accommodate the observed asymmetrical nature of friction in the motor [Wang, 1987], kinetic friction is modelled in AEC I as follows:

$$T_f = \alpha_1 \left(\frac{sgn(\dot{\theta}_p) + 1}{2} \right) + \alpha_2 \left(\frac{sgn(\dot{\theta}_p) - 1}{2} \right) , \tag{6}$$

where α_1 and α_2 represent the magnitude of kinetic friction in the positive and negative directions, respectively.

While Gilbart and Winston used only proportional feedback control in addition to the adaptive control, our controller uses a control input based on the computed torque method with integration in addition to the adaptive control. Figure 3 shows the block diagram for AEC I. A stability analysis of this controller which follows [Gilbart and Winston, 1974] and employs Lyapunov's direct method yields the result that $(e, \dot{e}) = (0, 0)$ is an asymptotically stable equilibrium point where $\dot{e} = \dot{\theta}_m - \dot{\theta}_p$, $e = \theta_m - \theta_p$ and $\dot{\theta}_m$ and θ_m are the ideal model velocity and position, respectively. Details are to be found in [Ehrich, 1991].

The second controller (referred to as AEC II) is based on the method developed by [Craig, 1988] in his design of an adaptive robotic manipulator controller. As in the work of Gilbart and Winston, Craig used an MRAC approach and assumed the classical, symmetrical model of kinetic plus viscous friction. Four different versions of the AEC II controller are developed, each with a different model of friction. For reference, we solve equation (5) for input u and rewrite as

$$u = (1/c_3)\ddot{\theta}_p + (c_1/c_3)\dot{\theta}_p + (c_2/c_3)T_f = (1/c_3)\ddot{\theta}_p + Q \ . \tag{7}$$

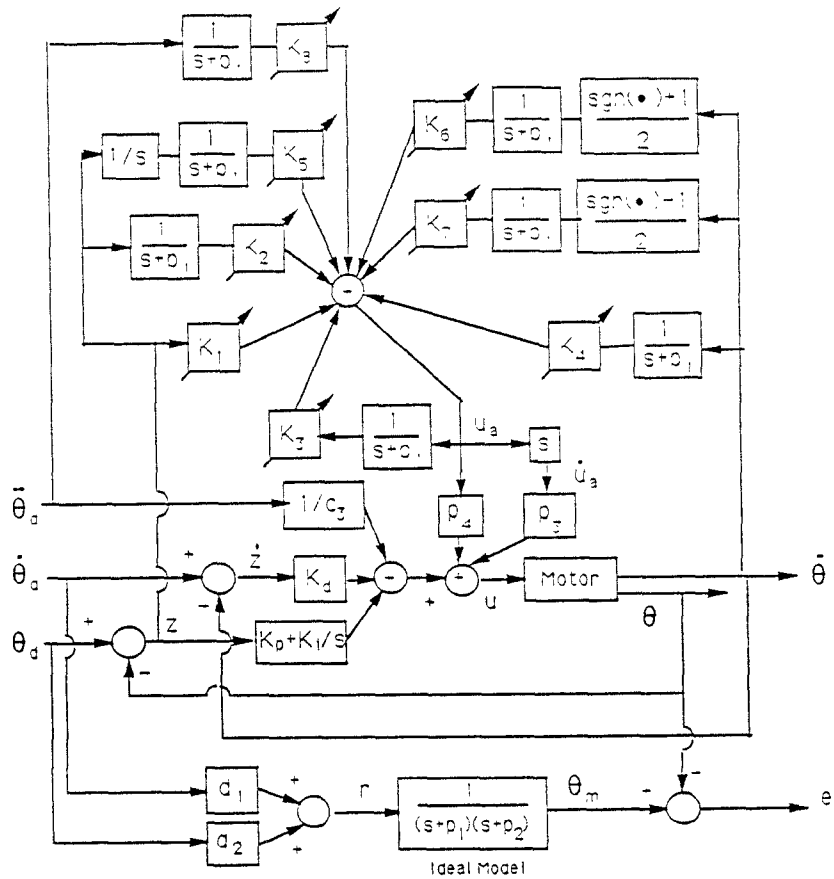

Figure 3: AEC I

Friction model (a) is the simple kinetic plus viscous friction model used by Craig in his design such that

$$Q^{(a)} = p_1\dot{\theta}_p + p_2 sgn(\dot{\theta}_p) \ , \tag{8}$$

where p_1 and p_2 are the unknown parameters. Model (b) assumes the asymmetric kinetic plus viscous friction model represented by

$$\begin{aligned} Q^{(b)} &= p_1\dot{\theta}_p\tfrac{1+sgn(\dot{\theta}_p)}{2} + p_2\dot{\theta}_p\tfrac{1-sgn(\dot{\theta}_p)}{2} \\ &\quad + p_3\tfrac{sgn(\dot{\theta}_p)+1}{2} + p_4\tfrac{sgn(\dot{\theta}_p)-1}{2} \ , \end{aligned} \tag{9}$$

where p_1 and p_2 are the unknown viscous friction parameters in the positive and negative directions, respectively and p_3 and p_4 are the unknown kinetic friction parameters in the positive and negative directions, respectively.

Model (c) includes a linear model of Stribeck friction in addition to kinetic plus viscous friction. Stribeck friction can be modelled according to (4) for

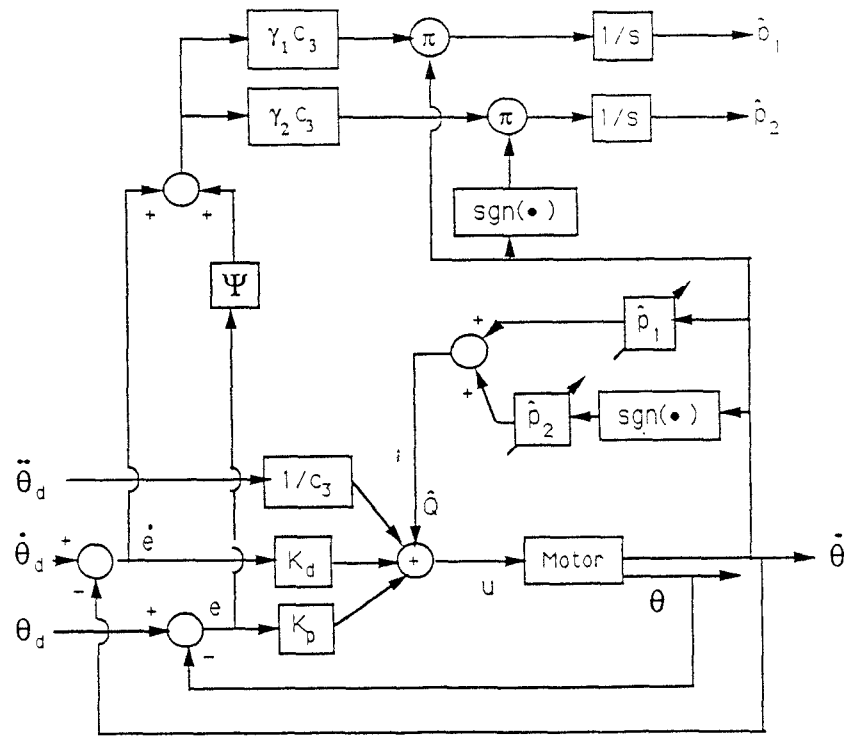

Figure 4: AEC II

$V = \dot{\theta}_p$ and $V_{str} = \dot{\theta}_{str}$. However, AEC II requires dynamics that are linear in the unknown parameters. To derive a linear-in-parameters model, the exponential in (4) is replaced by its Taylor series approximation which yields

$$Q^{(c)} = p_1\dot{\theta}_p + p_2 sgn(\dot{\theta}_p) + p_3\dot{\theta}_p{}^2 sgn(\dot{\theta}_p) \; . \tag{10}$$

For comparative purposes, Model (d) includes kinetic plus viscous plus Stribeck friction terms according to the linearized model of [Canudas de Wit, 1989] such that

$$Q^{(d)} = p_1\dot{\theta}_p + p_2 sgn(\dot{\theta}_p) + p_3|\dot{\theta}_p|^{1/2} sgn(\dot{\theta}_p) \; . \tag{11}$$

The block diagram for AEC II is shown in Figure 4. A stability analysis that follows [Craig, 1988] and uses the Kalman-Yakubovich Lemma and Lyapunov's

direct method shows that $(e, \dot{e}) = (0, 0)$ where $\dot{e} = \dot{\theta}_d - \dot{\theta}_p$ and $e = \theta_d - \theta_p$ (see [Ehrich, 1991]).

The third controller, AEC III, is an estimation-based controller that follows the work of [Walrath, 1984] described in the previous section. From experimental results, Walrath postulated the following first-order model of the bearing friction T_f:

$$\tau \frac{dT_f}{dt} + T_f = T_c sgn(\dot{\theta}_p) \tag{12}$$

where T_c is the rolling bearing friction (i.e. kinetic friction) and τ is a time constant. Clearly (12) is a rewriting of the Dahl friction model of (3) with $i = 1$ and replacing F_f with T_f, F_{f_c} with T_c and x with θ_p where

$$\tau = \frac{T_c}{\sigma |\dot{\theta}_p|} . \tag{13}$$

Walrath incorporated the friction model (12) into his controller by using it to predict friction torque. He empirically determined the value of τ for a given control experiment by repeating the experiment many times, each time varying only τ, until the optimum τ was found, i.e., the τ that yielded the minimum stabilization error. Based on optimum τ values (τ_{opt}) calculated for a range of operating conditions, Walrath empirically derived a linear prediction of τ_{opt} as a function of the inverse of the RMS system acceleration $\ddot{\theta}_{rms}$. This is *inconsistent* with Dahl's model which predicts that τ is inversely proportional to velocity (13).

On the other hand, a *consistent* relationship for τ was found for the electric motor of the present study. Experiments similar to Walrath's were performed on the motor to determine τ as a function of operating conditions. Figure 5(a) shows the results of one of the experiments. RMS angular position error is plotted against $\omega = 1/\tau$ for sinusoidal trajectory tracking with trajectory frequency $f = 0.25$ Hz and amplitude $A = 0.25$ rad. Each point on the plot represents a single repetition (320 seconds long) of the experiment. The optimal

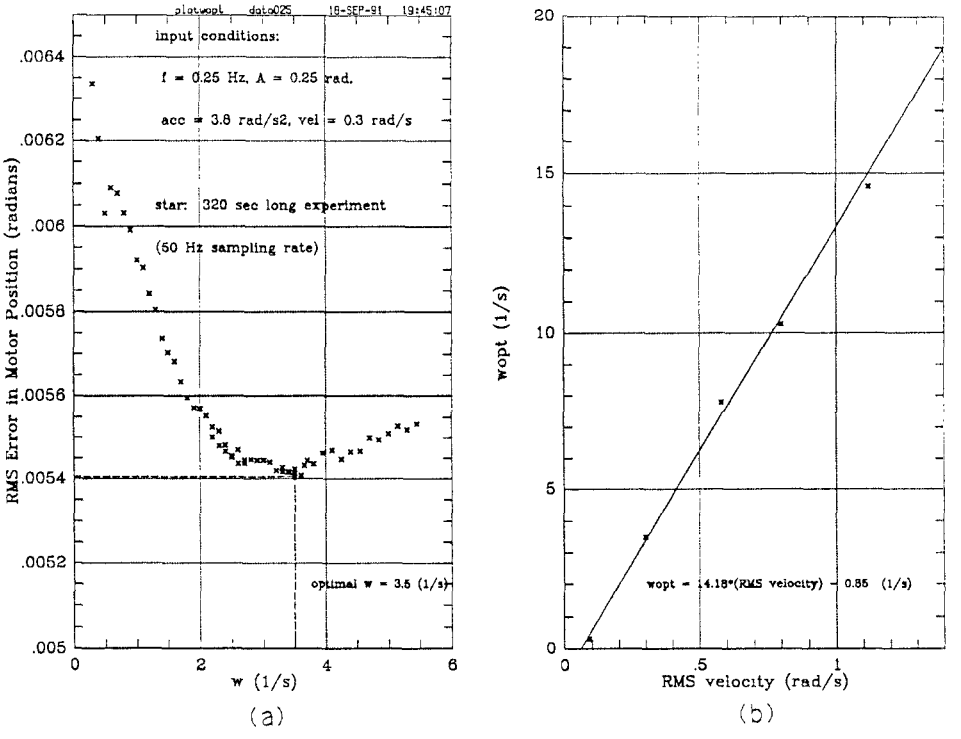

Figure 5: (a) Experimental Results Used to Determine Optimal ω ($f = 0.25$ Hz) and (b) Optimal Values of ω as Function of Operating Conditions

ω (ω_{opt}) was selected to correspond to the minimum RMS error. Figure 5(b) plots ω_{opt} for all the experiments as a function of RMS velocity and shows ω_{opt} to be a linear function of RMS velocity.

Additionally, while Walrath's controller only used proportional feedback control in conjunction with the friction compensation, AEC III uses feedback control based on the computed torque method with integration. Figure 6 shows a block diagram of AEC III.

Since Walrath did not provide a stability analysis for his controller, an original stability analysis has been developed based on the passivity formalism. Consider AEC III with derivative feedback only. Let the forward part of the loop including the motor, friction prediction and derivative gain K_d be represented by H_1. The feedback part of the loop is represented by H_2 which implies that $H_2 = 1$ from Figure 6. Then it follows from [Hill and Moylan, 1977], that

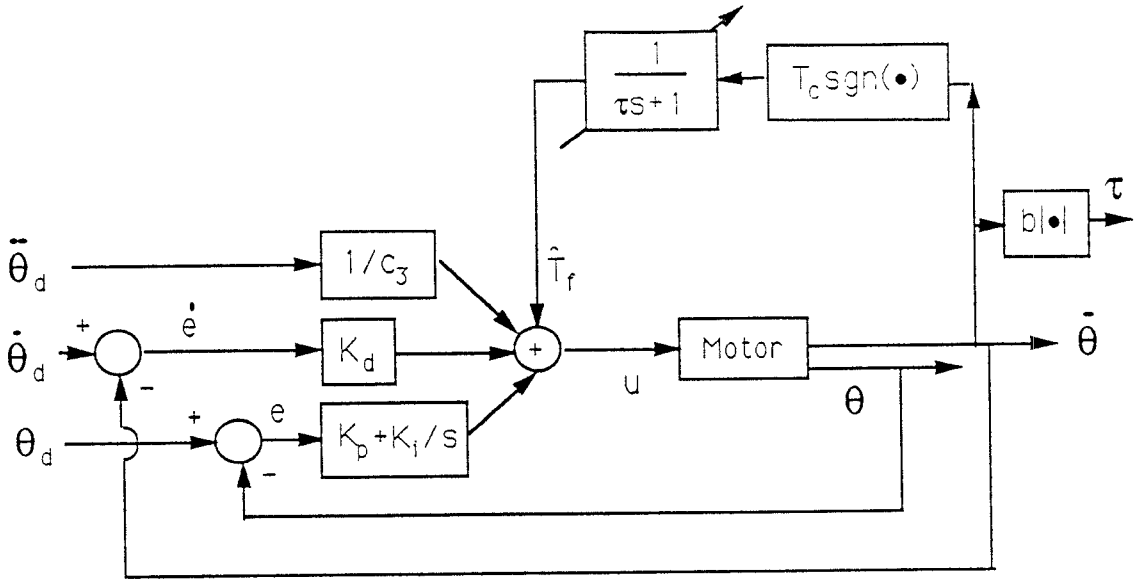

Figure 6: AEC III

if both H_1 and H_2 are Y-strongly passive (YSP), the feedback system is asymptotically stable. The fact that H_2 is SPR implies that H_2 is YSP. It remains to prove that H_1 is YSP.

System H_1 can be described by the following equations:

$$\ddot{\theta}_p + c_1\dot{\theta}_p = -c_2 T_f + c_2\hat{T}_f + c_3 K_d \dot{e} \ , \tag{14}$$

$$\dot{T}_f = -b|\dot{\theta}_p|T_f + bT_c\dot{\theta}_p \ , \tag{15}$$

$$\dot{\hat{T}}_f = -\hat{b}|\dot{\theta}_p|\hat{T}_f + \hat{b}T_c\dot{\theta}_p \ . \tag{16}$$

where the $\hat{}$ indicates a predicted value and we have assumed $\omega = b|\dot{\theta}_p|$ and $\hat{\omega} = \hat{b}|\dot{\theta}_p|$.

Define the state $(x_1, x_2, x_3, x_4) = (\theta_p, \dot{\theta}_p, T_f, \hat{T}_f)$ and let $u = \dot{e}$. Now define $\phi : \mathcal{R}^4 \mapsto \mathcal{R}$ as

$$\begin{aligned}\phi(x) \ = \ & \tfrac{c_2}{c_3 K K_d}[\tfrac{K}{2c_2}{x_2}^2 + x_3(x_1 - \gamma_1/b) - \tfrac{1}{2}T_c b(x_1 - \gamma_1/b)^2 + \textstyle\int bx_1x_3|x_2| \\ & + x_4(x_1 - \gamma_2/\hat{b}) - \tfrac{1}{2}T_c\hat{b}(x_1 - \gamma_2/\hat{b})^2 + \textstyle\int \hat{b}x_1x_4|x_2|]\end{aligned} \tag{17}$$

where K, γ_1, and γ_2 are constants to be defined later. Differentiating (17) with respect to time yields the supply rate

$$\dot{\phi}(x) = uy - \epsilon y^2 \,. \tag{18}$$

where $\epsilon = c_1/c_3 K_d > 0$ and γ_1, γ_2, and K are chosen appropriately for the two cases $x_2 = \dot{\theta}_p \geq 0$ and $x_2 = \dot{\theta}_p \leq 0$.

For $x_2 = \dot{\theta}_p \geq 0$ (or $x_2 = \dot{\theta}_p \leq 0$), $x_1 x_3 = T_f \theta_p \geq 0$ and $x_2 x_4 = \hat{T}_f \theta_p \geq 0$. Additionally, x_1 and x_3 are both bounded since $0 \leq x_1 = \theta_p \leq 2\pi$ and $-T_c \leq x_3 = T_f \leq T_c$. Therefore $\phi(\cdot)$ from (17) is bounded below. Define C as the greatest lower bound of $\phi(x)$. Then there exists some $x_0 \in \mathcal{R}^4$ such that $\phi(x_0) = C$. Next define $\check{\phi} : \mathcal{R}^4 \mapsto \mathcal{R}$ such that

$$\check{\phi}(y) = \phi(y + x_0) - C \,. \tag{19}$$

Then $\check{\phi}(0) = 0$ and $\check{\phi}(y) \geq 0 \ \forall y$ and $\dot{\check{\phi}}(y) = \dot{\phi}(y)$. Thus, according to [Hill and Moylan, 1977] H_1 is YSP and the feedback system of AEC III is input-output asymptotically stable. This implies that $\dot{\theta}_p$ will follow $\dot{\theta}_d$.

4 Experimental Program and Results

The experimental system consisted of a direct-drive, brush-type dc motor, angular position and velocity sensors, a power amplifier, an IBM AT PC, and supporting hardware and software for communication and control. The IBM PC was used to control the operation of the motor. A 50 Hz sampling rate was used throughout the experimental program.

Angular position of the motor was measured by a 12 bit absolute optical shaft encoder. The position data was transmitted to the PC with a measurement resolution of 0.00154 radians (0.088 degrees). A tachometer measured the angular velocity of the motor with a resolution of 0.012 rad/s.

The motor system was modelled according to (5) where u is the input voltage to the motor. For system simulations. friction was modelled as symmetric kinetic plus viscous friction. The friction parameters, assumed to be constant, were measured in previous work by [Wang, 1987]. The motor model was successfully verified by comparing results of voltage pulse experiments on the motor to results of identical simulated experiments on the motor model.

The motor model along with a simulation of a standard PID controller was then used to design an optimized benchmark PID controller for position tracking. The PID controller gains were selected to optimize the motor response to a 0.25 radian step demand in angular position. CONSOLE, a numerical optimization tool described in [Fan et al., 1987], was used to perform the optimization. Two functional objectives were specified, one to minimize the overshoot of the step response and one to maximize the rise of the step response. The effectiveness of the optimized gains was verified by a 0.25 radian step experiment on the motor.

The experimental program on the electric motor consisted of comparative position trajectory tracking tests using five different controllers: AEC I, II, III, a controller with dither and the optimized benchmark PID controller. The controller with dither was implemented identically to the PID controller except that a dither signal was added to the control input. The frequency of the dither signal was 25 Hz which is the maximum possible given the 50 Hz sampling rate. The amplitude of the dither signal was more than twice the magnitude of the static friction.

In each experiment the motor was required to track a sinusoidal position trajectory such that:

$$\theta_d = Asin(2\pi ft) \tag{20}$$

where A is the amplitude and f the frequency of the demanded trajectory.

This required sinusoidal motion provided a useful means for investigating friction compensation since the motor was forced to repeatedly pass through zero velocity where friction behavior is most difficult to control. The sinusoidal motion also provided a reasonably realistic scenario since manipulators are often required to perform repetitive tasks that demand sinusoidal joint motions.

The sinusoidal trajectories tracked in the experimental program ranged in frequency f from 0.1 Hz to 1.0 Hz. The lower limit of this range was selected to minimize motor velocity and to avoid large errors due to velocity measurement resolution. The upper limit of this range was selected to maximize motor velocity without generating gross errors due to the limitations of the 50 Hz sampling rate. A 0.25 radian amplitude A was used for all sinusoidal trajectory tracking experiments.

The RMS position error for each of the controllers and each experiment is listed in Table 1. Each RMS position error is calculated based on 16 seconds (800 samples) of data. As indicated in Table 1, the controller with dither does not significantly improve the tracking performance as compared to the benchmark PID controller. This is due to the fact that the dither frequency is limited to 25 Hz. AEC I, II, and III, on the other hand, all effectively improved tracking performance for the range of sinusoidal trajectory frequencies tested. The lower values of percent reduction in RMS error for the 0.1 Hz experiment are most likely due to the resolution of the position measurements.

Figures 7, 8, and 9 show the absolute value of PID controller position error compared to the position error from AEC I, II, and III, respectively. In each case the PID controller result is shown in a solid line and the nonlinear controller result is shown in a dashed line. Note that the two seconds (100 samples) shown correspond to the first two seconds of the experimental results beginning at the time listed in the fourth column of Table 1.

Type of Controller	Trajectory Frequency f (Hz)	RMS Position Error (rad)	Time Elapsed Before Error Calculated (s)	% Error Reduction from PID
PID	1.0	0.0106	0	-
Dither	1.0	-	-	-
AEC I	1.0	0.0048	400	55
AEC II	1.0	0.0079	12	25
AC III	1.0	0.0054	12	49
PID	0.5	0.0069	0	-
Dither	0.5	0.0066	0	4
AEC I	0.5	0.0033	400	52
AEC II	0.5	0.0041	12	41
AEC III	0.5	0.0028	12	59
PID	0.25	0.0063	0	-
Dither	0.25	0.0055	0	13
AEC I	0.25	0.0043	400	32
AEC II	0.25	0.0037	12	41
AEC III	0.25	0.0036	12	43
PID	0.1	0.0060	0	-
Dither	0.1	0.0045	0	25
AEC I	0.1	-	-	-
AEC II	0.1	0.0044	12	27
AEC III	0.1	0.0040	12	33

Table 1: Results of Sinusoidal Tracking Experiments

A comparison of these plots and the performance results of Table 1 suggests that AEC II is not as effective at friction compensation as AEC III. This can be explained by noting that there are a couple of relatively large error peaks in Figure 9 for AEC II. These occur because AEC II overcompensates when friction changes instantaneously. The large error peaks seen in Figure 11 correspond in time to the instantaneous friction changes. This overcompensation and corresponding large error indicates that the classical friction model does not describe friction during transient velocity reversals as well as the Dahl model.

The numbers listed in Table 1 are averages of results from experiments made over a period of a few days. However, over the course of about six months

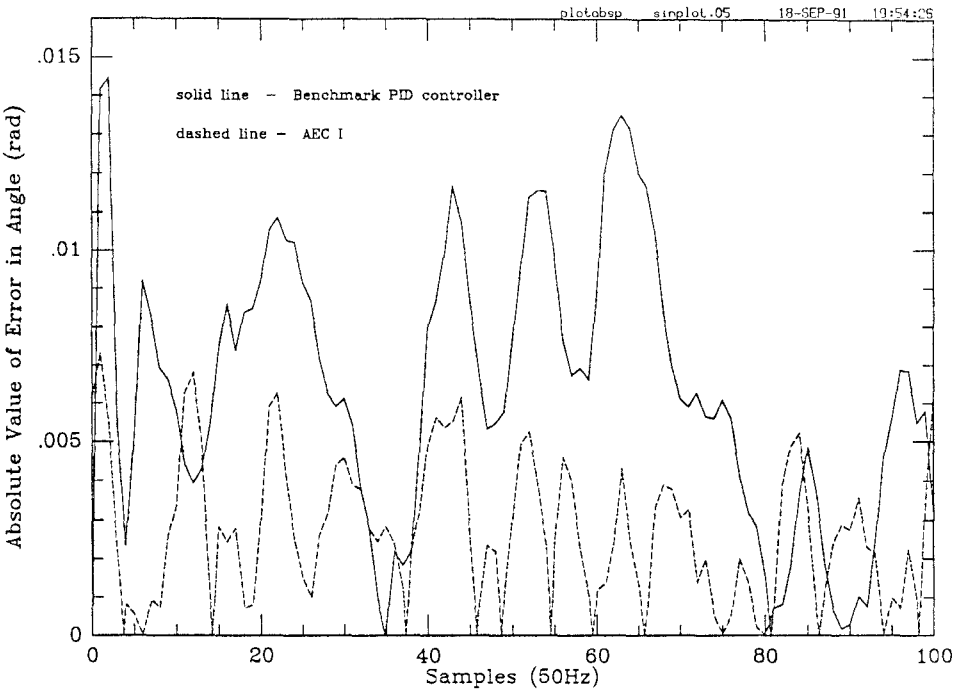

Figure 7: Position Error for AEC I Compared to Benchmark PID Controller

during which these experiments were performed, there was a great deal of repeatability in the percent reduction in RMS position error achieved by the two adaptive controllers. The experiments were run during different seasons and during different stages of motor "warm-up" such that friction parameters may have varied from experiment to experiment due to temperature differences. Additionally, over the six month period the friction parameters may have changed due to system aging. The fact that the adaptive controllers were consistently effective under these varying conditions provides evidence for the effectiveness of the adaptability of these controllers.

The results for AEC II provided in Table 1 correspond to experiments performed using Model (a) friction. Experiments using Model (b) friction showed an insignificant change in performance. This result indicates that for this set of experimental conditions, additional adaptive terms to account for friction

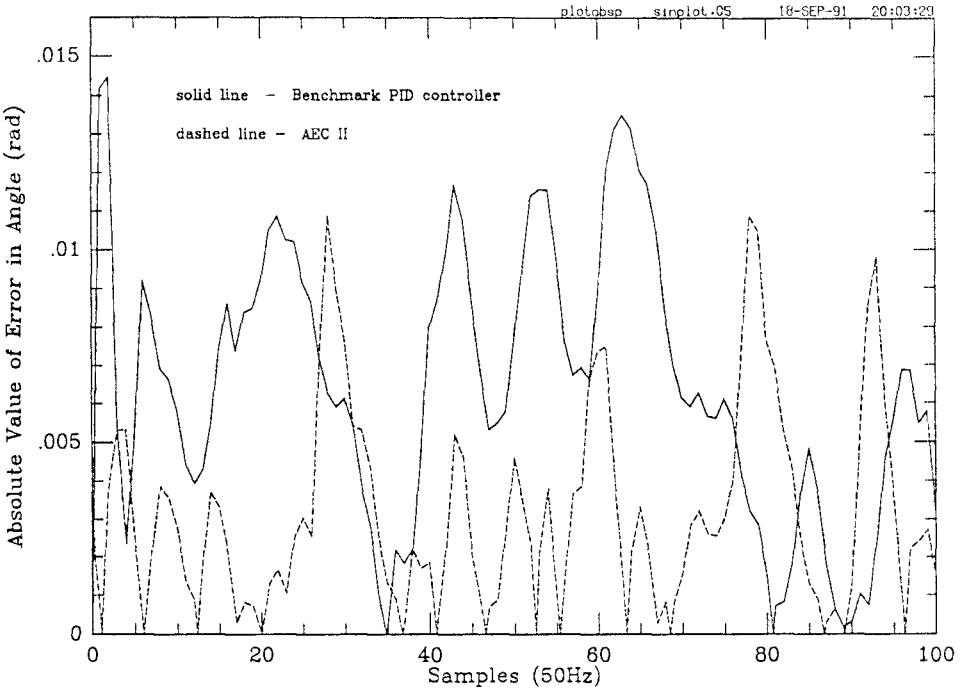

Figure 8: Position Error for AEC II Compared to Benchmark PID Controller

asymmetries are not necessary. Experiments using Models (c) and (d) for friction showed only a slight improvement in performance as compared to the Model (a) experiments. Since the additional friction terms in Model (c) and Model (d) were intended to account for Stribeck friction, this result can be attributed to the fact that Stribeck friction is probably not completely measured by the experimental system since the critical Stribeck velocity may be approximately of the same or lower order as the velocity measurement resolution.

The main disadvantage associated with AEC I was its excessively slow rate of adaptation. Although tracking performance began to improve immediately, it was not until 400 seconds into the experiment that the best results were achieved.

AEC II had the disadvantage that for the implementation that yielded the best results, the adaptive parameters tended to drift and performance deteriorated after a while. This could be avoided by resetting the parameters when

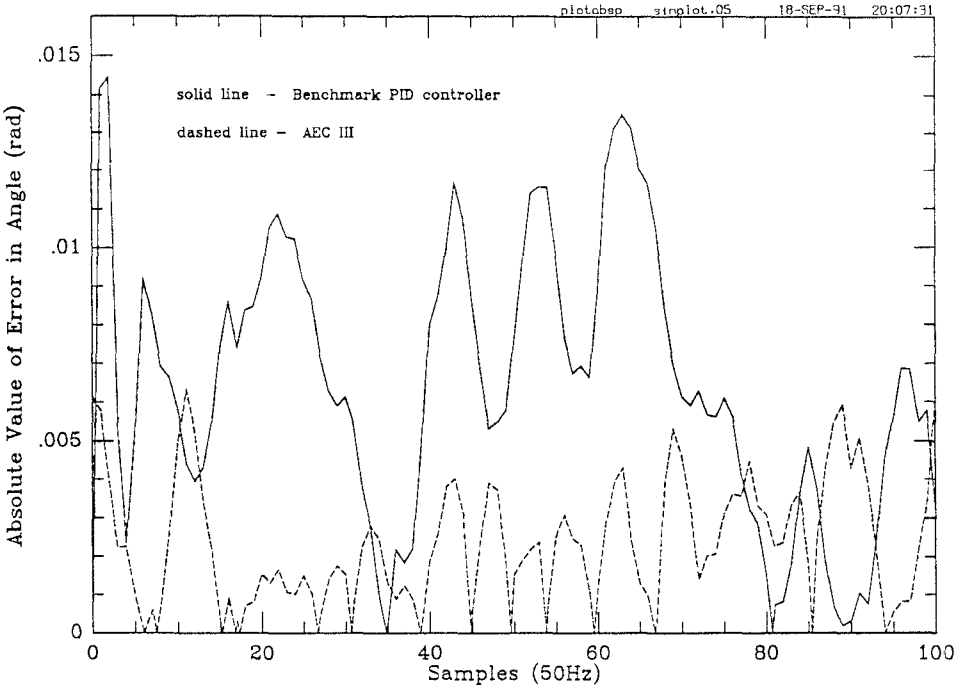

Figure 9: Position Error for AEC III Compared to Benchmark PID Controller

they went out of a predefined range as suggested by [Craig, 1988].

AEC III, on the other hand, was very reliable and performed best of all the controllers. However, this controller is at a disadvantage in that it requires a lengthy experiment up front to determine the constants in the relationship between the friction time constant τ and the RMS velocity. Additionally, since kinetic friction T_c is held constant, AEC III is not best suited for adapting to changes in friction due to temperature or aging. This could be fixed, however, by adding an adaptive component to update T_c.

Finally, torque ripple in the motor adds a position-dependent component to the motor dynamics and could have affected how each of the controllers performed. All of the data in Table 1 applies to experiments run such that the initial position was 0.0 radians. However, it was observed that the performance of the controllers varied when different initial positions were used. To investigate this torque ripple effect, the experiment with $f = 0.5$ Hz was run again on

Initial Position (rad)	RMS Position Error with PID Controller (rad)	% RMS Position Error Reduction from PID	
		AEC II	AEC III
-2.698	0.0086	16	23
-2.484	0.0082	26	33
-2.075	0.0091	21	23
-1.546	0.0081	30	35
-1.080	0.0079	30	39
-0.709	0.0079	28	29
-0.261	0.0072	33	36
-0.069	0.0071	32	41
0.000	0.0067	34	52
0.086	0.0068	34	46
0.689	0.0060	28	42
1.172	0.0061	15	56
1.758	0.0066	18	39
2.484	0.0076	32	37
2.720	0.0074	22	39
Average	0.0074	27	38
Std. Dev.	0.00087	6.4	8.9

Table 2: Experimental Results at Different Initial Positions ($f = 0.5$ Hz)

the PID controller and AEC II and III at 15 different initial positions chosen randomly. The results of these experiments are shown in Table 2. According to these results, neither AEC II nor III performed on average as well as at an initial position of 0.0 radians. However, the greater effectiveness of AEC III relative to AEC II was observed at every initial position. From Table 2, it can be concluded that while torque ripple does affect somewhat the performance of these two adaptive controllers, it does not affect their relative effectiveness.

The effect of digital sampling rate on the performance of AEC II and III was also investigated by repeating the experiments of the experimental program with a 100 Hz sampling rate. Table 3 lists the results of these experiments. According to Table 3, the increased sampling rate did not have a dramatic effect on the performance of AEC III. However, AEC II performed significantly better with

Trajectory frequency f (Hz)	% RMS Position Error Reduction from PID			
	AEC II		AEC III	
	50 Hz	100 Hz	50 Hz	100 Hz
1.0	25	64	49	42
0.5	41	60	59	56
0.25	41	45	43	56
0.1	27	35	33	29

Table 3: Comparison of Tracking Experiment Results with 50 Hz and 100 Hz Sampling Rates

the 100 Hz sampling rate than with the 50 Hz sampling rate, particularly for experiments with $f = 0.5$ Hz and $f = 1.0$ Hz. This improved performance may be explained by the fact that overcompensation provided by AEC II for instantaneous changes in friction is not as prolonged with a 100 Hz sampling rate as it is with a 50 Hz sampling rate. Based on the results of Table 3, one can conclude that the relative effectiveness of AEC II and III is greatly affected by the digital sampling rate.

5 Conclusions

In this paper a comprehensive investigation was presented of control strategies for friction compensation in servomechanisms performing low-velocity position tracking. The major conclusions of the investigation are as follows:

- AEC I, II, and III all provide improved servomechanism position control compared to an optimized PID controller and controller with (limited frequency) dither for low-frequency sinusoidal position trajectory tracking experiments on a direct-drive dc motor. Additionally, the experimental results of this paper coupled with the results of [Gilbart and Winston, 1974, Craig, 1988, Walrath, 1984] provide evidence for the general applicability

of these adaptive and estimation-based controllers.

- The Dahl model provides a realistic and reliable model of friction, particularly during sinusoidal motion of the mechanism. Evidence for this can be found (1) in the fact that the empirically derived model of the friction time constant τ as a linear function of velocity is consistent with Dahl's original model and (2) by the relatively high effectiveness of AEC III which is based on the Dahl model. This conclusion is noteworthy since friction is typically considered to behave according to the classical friction model.

- Mechanical considerations such as torque ripple and digital sampling rate play an important role in the performance of the adaptive and estimation-based controllers.

Further research should be pursued to understand the relationship between the classical friction model and the Dahl friction model. A determination of how to link the Dahl model of pre-sliding displacements with the classical model of sticking and sliding would provide a more complete and cohesive understanding of friction that could potentially be used to improve friction-compensating control strategies.

6 Acknowledgements

It is a pleasure to acknowledge numerous stimulating discussions on the subject of friction with Josip Lončarić. The first author is also grateful for the graduate fellowship support received from the University of Maryland Graduate School and Systems Research Center.

References

[Armstrong-Hélouvry, 1991] Armstrong-Hélouvry, B., *Control of Machines with Friction,* Kluwer Academic Publishers, Boston, 1991.

[Canudas de Wit, 1989] Canudas de Wit, C., Experimental results on adaptive friction compensation in robotic manipulators: low velocities, in *Lecture Notes in Control and Information Sciences, 139,* edited by V. Hayward and O. Khatib, pp. 196–214, Springer-Verlag, 1989.

[Canudas et al., 1986] Canudas, C., K. Astrom, and K. Braun, Adaptive friction compensation in dc motor drives, in *Proceedings of the 1986 International Conference on Robotics and Automation,* pp. 1556–1561, IEEE, San Francisco, CA, April 1986.

[Courtney-Pratt and Eisner, 1957] Courtney-Pratt, J. and E. Eisner, The effect of a tangential force on the contact of metallic bodies, *Proceedings of the Royal Society, A238,* 529–550, 1957.

[Craig, 1988] Craig, J., *Adaptive Control of Mechanical Manipulators,* Addison-Wesley, Reading, MA, 1988.

[Dahl, 1977] Dahl, P., Measurement of solid friction parameters of ball bearings, in *Proceedings of the 6th Annual Symposium on Incremental Motion, Control Systems and Devices,* pp. 49–60, University of Illinois, 1977.

[Ehrich, 1991] Ehrich, N. E., *An Investigation of Control Strategies for Friction Compensation,* Master's Thesis 91-4, Systems Research Center, U. of Maryland, College Park, MD, 1991.

[Fan et al., 1987] Fan, M., L. Wang, J. Koninckx, and A. Tits, *CONSOLE Users Manual,* Technical Report 87-212, Systems Research Center, 1987.

[Gilbart and Winston, 1974] Gilbart, J. W. and G. C. Winston, Adaptive compensation for an optical tracking telescope, *Automatica, 10,* 125–131, 1974.

[Hess and Soom, 1990] Hess, D. P. and A. Soom, Friction at a lubricated line contact operating at oscillating sliding velocities, *Journal of Tribology, 112,* 147–152, January 1990.

[Hill and Moylan, 1977] Hill, D. and P. Moylan, Stability results for nonlinear feedback systems, *Automatica, 13,* 377–382, 1977.

[Rabinowicz, 1965] Rabinowicz, E., *Friction and Wear of Materials,* John Wiley and Sons, 1965.

[Rice and Ruina, 1983] Rice, J. and A. Ruina, Stability of steady frictional slipping, *Journal of Applied Mechanics, 50,* 343–349, June 1983.

[Walrath, 1984] Walrath, C., Adaptive bearing friction compensation based on recent knowledge of dynamic friction, *Automatica, 20,* 717–727, 1984.

[Wang, 1987] Wang, L., *Control System Design for a Flexible Arm,* Master's Thesis 87-164, Systems Research Center, U. of Maryland, College Park, MD, 1987.